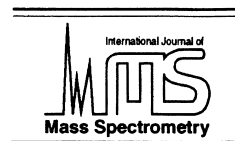




ELSEVIER

International Journal of Mass Spectrometry 209 (2001) 31–38



Improvement of detection limit for secondary-ion mass spectrometry depth profiling of argon in silicon by energy filtering

Hideyuki Yamazaki*

Toshiba Corporation, Research and Development Center, 8 Shinsugita-cho, Isogo-ku, Yokohama 235-8522, Japan

Received 22 September 2000; accepted 24 April 2001

Abstract

Secondary-ion mass spectrometry depth profiling of argon in Si has been investigated to achieve a lower detection limit. Depth profiling was performed by monitoring M^+ or MCs^+ secondary ions (M is the element to be analyzed), which were obtained with O_2^+ or Cs^+ primary ions, respectively. The influence of carbonaceous mass interference ions on the detection of argon was clarified and described. It was confirmed that almost all Ar^+ ions are formed in the vacuum within a distance of 100 μm from the sample surface, whereas the carbonaceous ions are formed at the surface. Using the energy-filtering (the sample voltage offsetting) technique, the detection of Ar^+ ions formed above the surface and of those formed at the surface leads to increasing detecting sensitivity. The energy-filtering technique can also eliminate the influence of carbonaceous mass interference ions during analysis of Ar^+ . The secondary-ion mass spectrometry technique using O_2^+ primary ions combined with the energy filtering provides a better detection limit for depth profiling of argon in Si than does Cs^+ primary-ion bombardment measurement. (Int J Mass Spectrom 209 (2001) 31–38) © 2001 Elsevier Science B.V.

Keywords: Secondary-ion mass spectrometry; Depth profiling analysis; Rare gases; Energy-filtering technique; Implantation

1. Introduction

Determination of trace elements and their depth distribution is a fundamental task for the development and production of various microelectronics products such as semiconductors, displays, and magnetic disk storage devices. Among surface analytical techniques, secondary-ion mass spectrometry (SIMS) is the most widely used tool because of its extreme sensitivity, high depth resolution, and ability to detect almost all elements [1–4]. However, the detection sensitivity

depends on the electron-exchange process between the sputtered atom and the surface [5–10]. This process is altered by the band structure of targets, the ejection velocity of secondary particles, and the atomic level of the sputtered atom. Therefore, if an element has high ionization potential or low electron affinity, it is difficult to obtain the high-ionization yield. For example, rare gas elements are known to have low ion yield. It has been reported that the detection limits of helium [11] and argon [12] are on the order of 10^{18} atoms/cm³ for depth profiles of He- or Ar-implanted Si and GaAs. It has also been demonstrated that monitoring of MCs^+ molecular ions (with M as the element to be analyzed) is

* E-mail: hideyuki.yamazaki@toshiba.co.jp

Table 1
Conditions of primary ion beam

Primary ion	Current density (mA/cm ²)	Ion current (μ A)	Raster size (μ m ²)	Beam size (μ m)
O ₂ ⁺	0.16	0.1	250 × 250	35
	0.48	0.3	250 × 250	40
	0.80	0.5	250 × 250	50
	1.25	0.5	200 × 200	50
	1.60	1.0	250 × 250	63
	2.00	1.2	250 × 250	70
	3.20	2.0	250 × 250	90
Cs ⁺	0.48	0.3	250 × 250	25
	0.80	0.5	250 × 250	33
	1.28	0.2	125 × 125	20
	2.00	0.2	100 × 100	20
	3.55	0.2	75 × 75	20
	4.00	0.1	50 × 50	15

advantageous for the analysis of rare gas elements and that the detection limits of argon [12] and helium [13] in Si are, respectively, $2 \times 10^{18} \text{ cm}^{-3}$ and $\sim 10^{19} \text{ cm}^{-3}$ for depth profiles of Ar- or He-implanted Si. However, few papers have been published on the comparison of detection limits for rare gas species obtained by analysis with O₂⁺ and Cs⁺ primary ions.

In this article, we report on a method to achieve a lower detection limit for depth profiling of argon in Si. First, we investigated the influence of carbon- and oxygen-containing mass interference ions on the detection of argon in Si. Next, the advantage of the energy-filtering technique is demonstrated. Finally, the detection limits of argon in Si obtained with an O₂⁺ primary-ion beam were compared with those obtained with a Cs⁺ primary-ion beam.

2. Experimental

The samples used were three types of implanted single-crystal (100) oriented Si wafers; 100 keV ⁴⁰Ar at a dose of $5 \times 10^{15} \text{ cm}^{-2}$, 80 keV ¹²C at a dose of $1 \times 10^{15} \text{ cm}^{-2}$, and 110 keV ¹⁶O at a dose of $1 \times 10^{15} \text{ cm}^{-2}$. To remove native oxide and organic contaminants, all Si wafers were chemically cleaned before implantation.

All the SIMS experiments were performed on a Cameca IMS-4f instrument. The mass-filtered O₂⁺ and

Cs⁺ primary ions with source potentials at 10 kV were employed. In the normal condition, the sample was held at +4.5 kV; an impact energy of an O₂⁺ or a Cs⁺ primary-ion beam was 5.5 keV, and secondary ions are accelerated to 4.5 kV. The sample potential can be varied between +4375 and +4625 V for recording energy distributions of positive secondary ions or for detecting secondary ions with the energy-filtering technique. The primary and secondary optics were adjusted for each voltage-offset condition. The primary beam was focused onto the sample surface. The value of the primary-ion current was monitored in the standard IMS-4f Faraday cup. The beam diameter is determined from the sidewall of the craters as measured by a Dektak 3030 profilometer between the 84% and 16% points [2]. The conditions of primary-ion current, raster size, primary-ion current density, and primary-ion beam size are summarized in Table 1. Positive secondary ions of M⁺ and MCs⁺ produced by an O₂⁺ and a Cs⁺ primary beam, respectively, were detected with electron multiplier. Depth profiles of argon that monitored Ar⁺ were obtained under various sample voltage-offset conditions. The secondary ions were collected from the central region of the sputtered craters to minimize the crater edge and sidewall effects. For all depth-profiling measurements, the energy window of the kinetic energy filter of secondary ions was symmetrically open to 55 eV

(total energy band pass of 110 eV). The energy window can be moved by ± 55 eV. Conversion of ion counts (count/s) to concentration (atoms/cm³) was accomplished using relative sensitivity factors (RSFs) [2,14]. The RSFs for each voltage-offset condition were determined from ion-implantation samples used in this experiment. The detection limits were defined as the average background signal at the constant level measured in the tail of the implantation profile. The kinetic energies of the secondary ions over a range of between -125 V and $+125$ V were determined by varying the sputtered ion-accelerating potential around $+4.5$ kV with a constant energy bandpass in the electrostatic sectors of the instrument.

All measurements were performed after 15 h pumping after sample introduction into the sample chamber. The vacuum in the sample chamber during the measurement was 2.7×10^{-7} Pa (2×10^{-9} Torr).

3. Results and discussion

3.1. Mass interference ions

During SIMS analysis of argon in Si, conceivable mass interference ions are $^{40}\text{(CSi)}^+$ and $^{40}\text{(C}_2\text{O)}^+$ for ^{40}Ar detection and $^{173}\text{(CSiCs)}^+$ and $^{173}\text{(C}_2\text{OCs)}^+$ for $^{173}\text{ArCs}^+$ detection, respectively. Origin of these ions is attributed to the residual gases in the SIMS instrument and to carbon and oxygen impurities present in the samples. Typical examples of SIMS depth profiles of $^{40}\text{(CSi)}^+$ and $^{173}\text{(CSiCs)}^+$ from $^{12}\text{C}^+$ implanted Si are shown in Fig. 1. The $^{40}\text{(CSi)}^+$ and $^{173}\text{(CSiCs)}^+$ were obtained by O_2^+ (ion-current density $J_{\text{O}_2^+} = 3.2$ mA/cm²) and Cs^+ (ion-current density $J_{\text{Cs}^+} = 2.0$ mA/cm²) primary-ion beam, respectively. Although the primary-ion current density of O_2^+ is higher than that of Cs^+ by a factor of 1.6, the erosion rate with a Cs^+ beam measurement is higher than that with O_2^+ . The reason is that the erosion rate with a Cs^+ beam is higher than that with an O_2^+ beam [2]. The surface peak in Fig. 1 is largely because of the presence of carbon contamination. Even if the difference in primary-ion current density between O_2^+

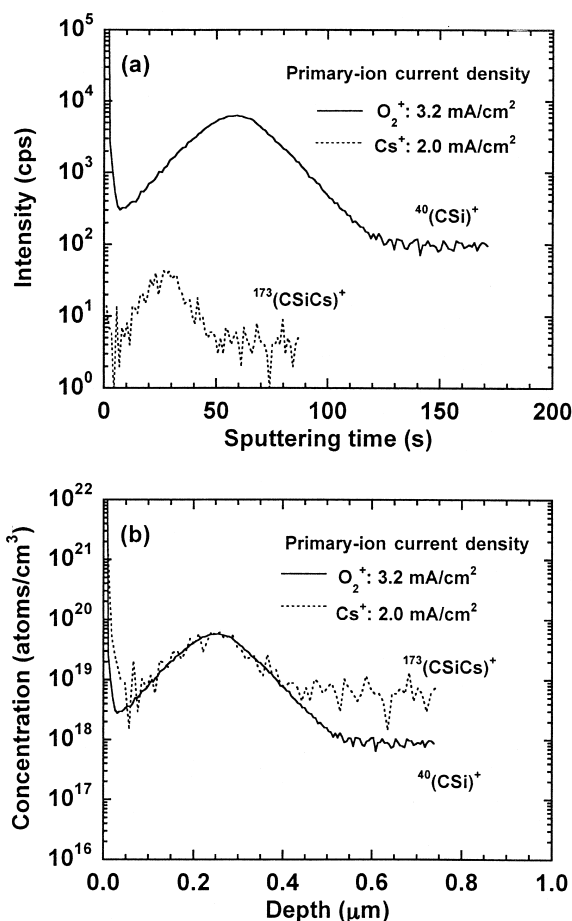


Fig. 1. Secondary-ion mass spectrometry depth profiles of a 150-keV ^{12}C implant in Si obtained by monitoring $^{40}\text{(CSi)}^+$ and $^{173}\text{(CSiCs)}^+$ ions; (a) raw data, (b) quantitative data.

and Cs^+ is considered, it is found that the secondary-ion intensity of CSi^+ is higher than that of CSiCs^+ . From Fig. 1b, one can see that the detection limits of CSi^+ and CSiCs^+ were 8×10^{17} and 5×10^{18} atoms/cm³, respectively. We also investigated the detection limits of $^{40}\text{(CSi)}^+$ and $^{173}\text{(CSiCs)}^+$, derived from ^{12}C -implanted Si sample, as a function of the primary-ion current density. The experimental results are presented in Fig. 2. The detection limits of CSi^+ became lower with increasing of O_2^+ primary-ion current density. However, the detection limits of CSiCs^+ were almost the same even if the primary-ion current density of Cs^+ was increased to 0.8 mA/cm²

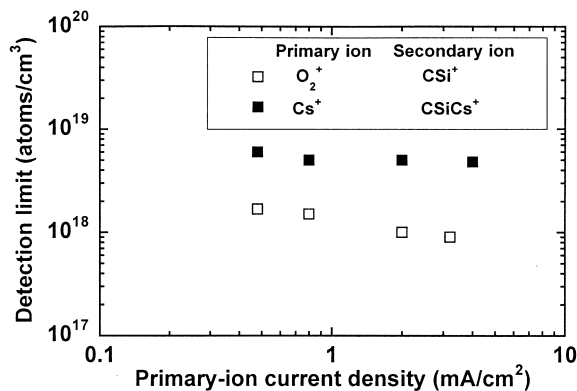


Fig. 2. Detection limit of carbon measured by monitoring $^{40}\text{CSi}^+$ and $^{173}\text{CSiCs}^+$ ions, obtained from measured depth profiles of an 80-keV ^{12}C implant in Si and plotted as a function of the O_2^+ and Cs^+ primary-ion current density, respectively.

or above. CSiCs^+ is found to be much less sensitive than CSi^+ .

Next, we consider the influence of mass interfer-

ence ions of $^{40}(\text{C}_2\text{O})^+$ and $^{173}(\text{C}_2\text{OCs})^+$. The primary-ion current density of 2.0 mA/cm^2 was selected for the investigation of $^{40}(\text{C}_2\text{O})^+$ and $^{173}(\text{C}_2\text{OCs})^+$ depth profiles. Fig. 3 shows the depth profiles of C_2O^+ and C_2OCs^+ obtained from ^{16}O -implanted Si wafer. The surface peak in the C_2O^+ profile is mainly attributable to the surface contamination arising from carbon and oxygen. According to SIMS depth profile, the peak concentration and depth for ^{16}O are $5 \times 10^{19} \text{ cm}^{-3}$ and $0.2 \mu\text{m}$, respectively. It is obvious that the implanted profiles of both C_2O^+ and C_2OCs^+ are not observed. We conclude that if the oxygen concentration in Si is $< 5 \times 10^{19} \text{ atoms/cm}^3$ and the carbon concentration in Si is $< 8 \times 10^{17} \text{ atoms/cm}^3$ (for O_2^+ primary-ion beam analysis) or $5 \times 10^{18} \text{ atoms/cm}^3$ (for Cs^+ primary-ion beam analysis), the influence of mass interference ions such as C_2O^+ and C_2OCs^+ is negligible. It was concluded that the formation of carbon-containing mass interference ions depends on

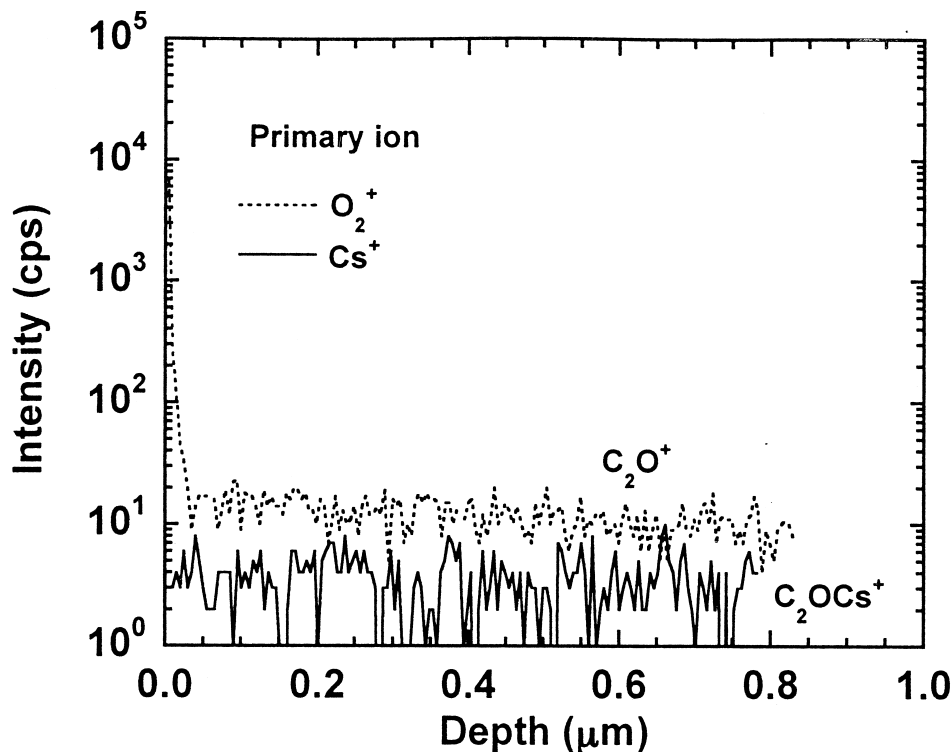


Fig. 3. Secondary-ion mass spectrometry depth profiles of a 150-keV ^{16}O implant in Si obtained by monitoring $^{40}(\text{C}_2\text{O})^+$ and $^{173}(\text{C}_2\text{OCs})^+$ ions.

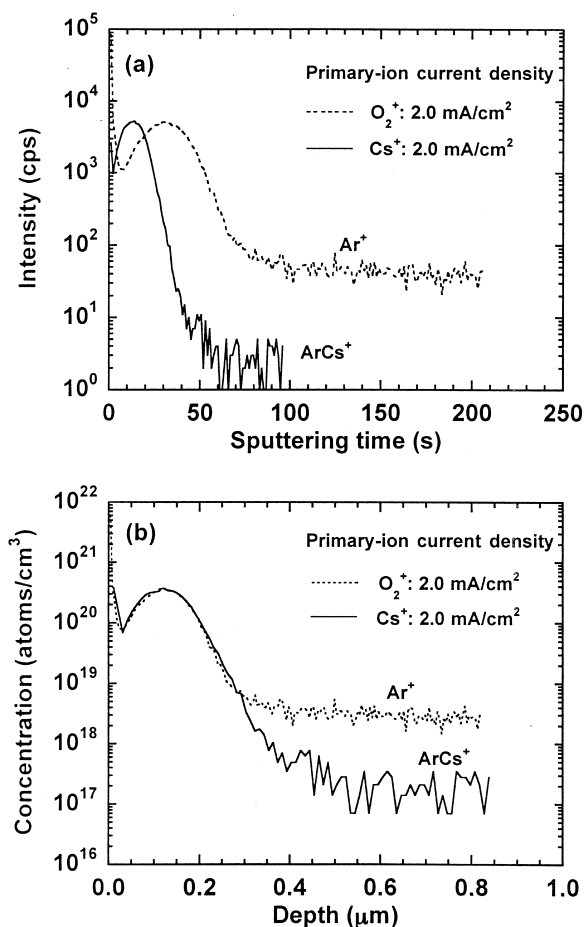


Fig. 4. Secondary-ion mass spectrometry depth profiles of a 100-keV ^{40}Ar implant in Si obtained by monitoring $^{40}\text{Ar}^+$ and $^{173}(\text{ArCs})^+$ ions; (a) raw data, (b) quantitative data.

both the amount of carbon and the primary-ion current density.

3.2. Depth profiles of Ar with O_2^+ or Cs^+ primary-ion beam

Examples of Ar^+ and ArCs^+ depth profiles from Ar implanted in Si are shown in Fig. 4. The Ar^+ and ArCs^+ were detected with O_2^+ ($J_{\text{O}_2^+} = 2.0 \text{ mA/cm}^2$) and Cs^+ ($J_{\text{Cs}^+} = 2.0 \text{ mA/cm}^2$) primary beam, respectively. As described in the previous section, it can be observed from Fig. 1a that the erosion rate with a Cs^+ beam is higher than that with an O_2^+ beam for the same current densities. The surface peak in the Ar^+

profile is primarily because of the carbon-containing mass interference ions resulting from carbon and oxygen contamination. It is seen from Fig. 4b that the detection limit of the ArCs^+ profile is lower than that of the Ar^+ profile. There is no difference in the depth resolution between the Ar^+ and ArCs^+ profiles.

Next, we compared the secondary-ion intensities of both Ar^+ and ArCs^+ as a function of primary-ion current density. The experimental results for ion intensities are shown in Fig. 5. It is confirmed that the secondary-ion intensities of Ar^+ and ArCs^+ increase with increasing primary-ion current density. A similar result has already been reported by Ray and coworkers [12]. It can also be seen from Fig. 5 that the secondary-ion intensities of Ar^+ and ArCs^+ measured at various primary-ion current density are almost the same. The difference in the detection limits between Ar^+ and ArCs^+ profiles may be ascribable to the degree of mass interference effect for each of the O_2^+ and Cs^+ primary beam measurements.

3.3. Energy-filtering technique

The sputtered species having high ionization potentials, such as rare gases, are ionized almost entirely by gas phase ionization processes that occur in a vacuum above the sample surfaces [15]. In contrast, the ionization of sputtered contaminants containing C and O must have taken place at the sample surfaces. To verify the difference in ionization mechanism between Ar^+ and molecular ions containing C and O, that is, CSi^+ and C_2O^+ , the energy spectra of these ions were examined. The results obtained with 5.5 keV O_2^+ primary ion are shown in Fig. 6. The energy spectrum of ArCs^+ ion under 5.5 keV Cs^+ bombardment is also shown in Fig. 6. This figure indicates that a considerable amount of Ar^+ is formed in the vacuum within a distance of 100 μm from sample surface by the gas phase ionization processes, whereas the ionization of CSi and C_2O occurs at the sample surfaces. It is reasonable to expect that, by increasing the accelerating voltage, the argon detection limits, with monitoring of Ar^+ , are improved effectively because of both the detection of both Ar^+ ions formed above the surface and those formed at the

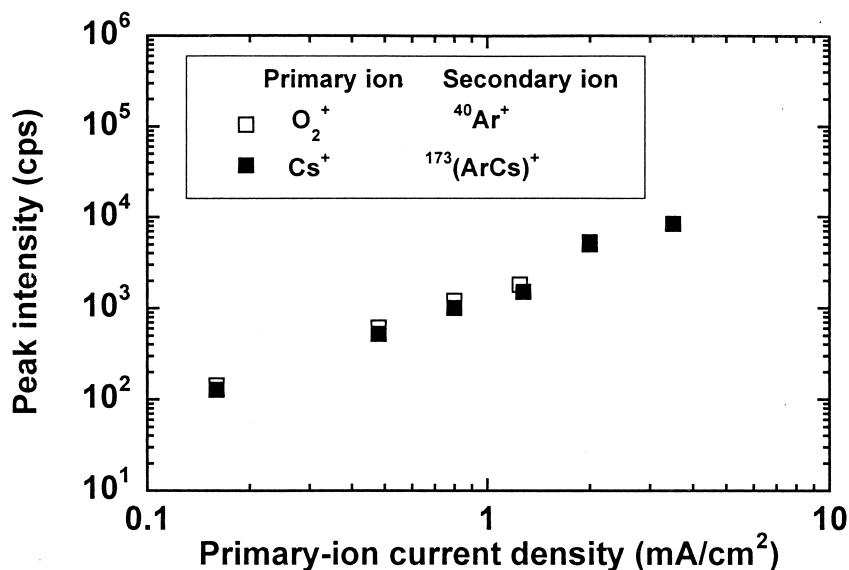


Fig. 5. Peak intensity of $^{40}\text{Ar}^+$ and $^{173}(\text{ArCs})^+$ ions, obtained from measured depth profiles of a 100-keV ^{40}Ar implant in Si and plotted as a function of the O_2^+ and Cs^+ primary-ion current density, respectively.

surface and, furthermore, the suppression of CSi^+ and C_2O^+ ions. Typical depth profiles of Ar^+ obtained with the energy-filtering technique are shown in Fig. 7. It is found that the surface peak stemming from carbon-contained mass interference ions disappears

with the increasing of sample offset voltage. To achieve a lower detection limit of Ar^+ , the optimum conditions for the energy-filtering technique were investigated as functions of energy window position and acceleration voltage. The results are shown in Fig.

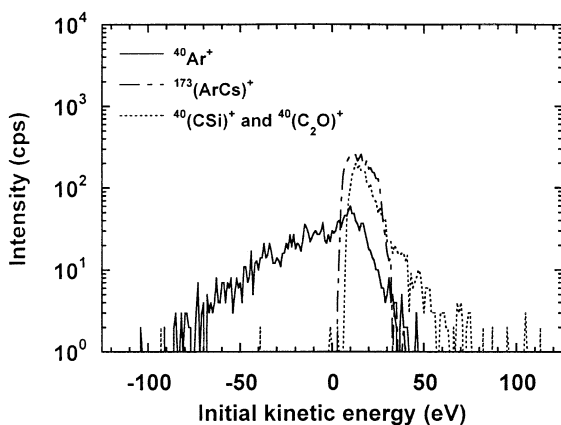


Fig. 6. Energy spectra of $^{40}\text{Ar}^+$, $^{40}(\text{CSi})^+$, $^{40}(\text{C}_2\text{O})^+$, and $^{173}(\text{ArCs})^+$. The secondary ions of Ar^+ and ArCs^+ were obtained from a 100-keV ^{40}Ar implant in Si. CSi^+ and C_2O^+ were done from an 80-keV $^{12}\text{C}^+$ implant in Si. O_2^+ and Cs^+ primary ions were, respectively, used for detection of $^{40}\text{Ar}^+$, $^{40}(\text{CSi})^+$, $^{40}(\text{C}_2\text{O})^+$, and $^{173}(\text{ArCs})^+$.

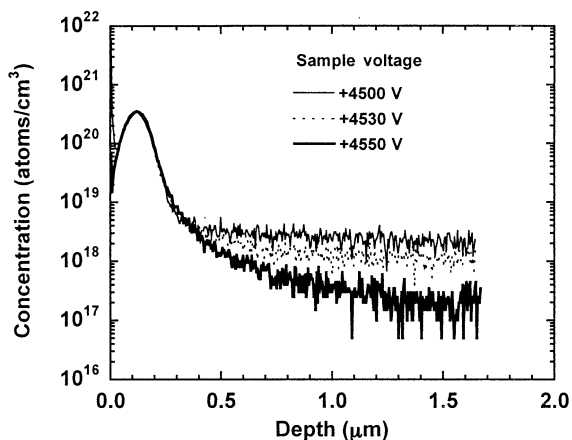


Fig. 7. Depth profiles of a 100-keV $^{40}\text{Ar}^+$ implant in Si monitoring of $^{40}\text{Ar}^+$. The Ar^+ profiles were obtained with various sample offset voltages (sample voltages): 0 (+4500 V), 30 (+4530 V), and 50 V (4550 V). The current density of the O_2^+ primary ion was 0.8 mA/cm².

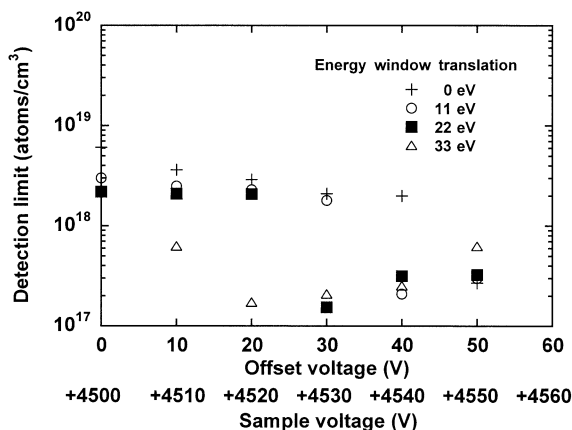


Fig. 8. Detection limit of argon in Si measured with various sample offset voltages and energy window translations toward the low-energy side. The secondary ions of $^{40}\text{Ar}^+$ were obtained with O_2^+ primary-ion at current density of 0.8 mA/cm^2 .

8. Compared with the case of using the normal analytical condition, it can be seen that the detection limit of argon is improved by approximately one order of magnitude by shifting energy of $\sim 50 \text{ eV}$. A similar effect can be achieved by translating the energy window toward lower energy side by 50 eV . No further improvement of detection limit was observed when energy distribution was shifted by $>60 \text{ eV}$ because of a loss of signal intensity. Next, we tried to apply the energy-filtering technique for the depth profiling of argon by monitoring ArCs^+ . As expected from Fig. 6, the energy filtering had no effect on the improvement of detection limits because the energy spectrum of ArCs^+ is very similar to those of CSi^+ and C_2O^+ , both in peak position and with high energy tails. Fig. 9 summarizes the argon-detection limits in Si obtained under various analytical conditions as a function of the primary-ion current density. Increasing the primary current density to $>4.0 \text{ mA/cm}^2$ for an O_2^+ or a Cs^+ beam did not result in the expected detection limit because of the crater edge and sidewall effects caused by a poorly focused primary beam.

It is concluded that using an O_2^+ primary-ion beam combined with the energy-filtering technique is the best analytical method to obtain good detection limit of argon in Si.

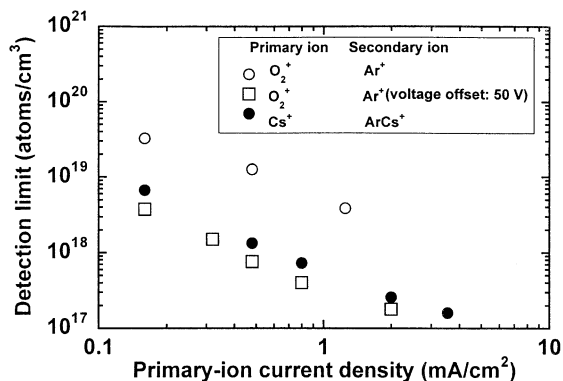


Fig. 9. Detection limits for argon measured by monitoring $^{40}\text{Ar}^+$, ^{40}Ar (sample offset voltage: 30 V), and $^{173}(\text{ArCs})^+$ ions, obtained from measured depth profiles in ^{40}Ar -implant silicon, plotted as a function of the O_2^+ and Cs^+ primary-ion current density, respectively.

4. Conclusion

During SIMS analysis of argon in Si, it has been shown that, in contrast to the $^{40}\text{Ar}^+$ ion-monitoring method, ArCs^+ is considerably less hindered by the interference from carbonaceous molecule ions such as CSi^+ and C_2O^+ . However, because of the differences in kinetic energy between Ar^+ and mass interference ions, the energy-filtering technique leads to improvement of the detection limits for Ar^+ by one order of magnitude. Detection limits for Ar^+ were found to be on the order of 10^{17} cm^{-3} at erosion rates of $\sim 1 \text{ nm/s}$. We conclude that monitoring Ar^+ in combination with energy filtering is a more useful technique for the analysis of argon in Si than is the ArCs^+ -monitoring method.

Acknowledgements

I thank one of referees for pointing out the ionization processes of Ar^+ and carbonaceous ions and the energy-filtering technique. I am grateful to Dr. M. Schuhmacher (CAMECA, Courbevoie, France) for providing a measurement method for actual energy band pass in the energy window and to A. Murakoshi (Semiconductor Company, Toshiba Corp.) for performing Ar implantations.

References

- [1] A. Benninghoven, F.G. Rüdenauer, H.W. Werner, *Secondary Ion Mass Spectrometry: Basic Concepts, Instrumental Aspects, Applications and Trends*, Wiley, New York 1987.
- [2] R.G. Wilson, F.A. Stevie, C.W. Magee, *Secondary Ion Mass Spectrometry: A Practical Handbook for Depth Profiling and Bulk Impurity Analysis*, Wiley, New York 1989.
- [3] M.G. Dowsett, E.A. Clark, in *Practical Surface Analysis*, 2nd ed., Vol. 2. Ion and Neutral Spectroscopy, D. Briggs, M.P. Seah (Eds.), Wiley, Chichester 1992, p. 229.
- [4] P.C. Zalm, *Rep. Prog. Phys.* 58 (1995) 1321.
- [5] J.K. Nørskov, B.I. Lundqvist, *Phys. Rev. B* 19 (1979) 5661.
- [6] M.L. Yu, *Phys. Rev. Lett.* 47 (1981) 1325.
- [7] N.D. Lang, *Phys. Rev. B* 27 (1983) 2019.
- [8] M.L. Yu, N.D. Lang, *Nucl. Instr. Meth. B* 14 (1986) 403.
- [9] M.L. Yu, *Nucl. Instr. Meth. B* 15 (1986) 151.
- [10] J. Los, J.J.C. Geerlings, *Phys. Rep.* 190 (1990) 133.
- [11] R.G. Wilson, V.R. Deline, C. G. Hopkins, *Appl. Phys. Lett.* 41 (1982) 929.
- [12] M.A. Ray, J.E. Baker, C.M. Loxton, J.E. Greene, *J. Vac. Sci. Technol. A* 6 (1988) 44.
- [13] H. Gnaser, H. Oechsner, *Surf. Interface Anal.* 17 (1991) 646.
- [14] R.G. Wilson, S.W. Novak, *J. Appl. Phys.* 69 (1991) 466.
- [15] M. Bernheim, G. Blaise, G. Slodzian, *Int. J. Mass Spectrom. Ion Phys.* 10 (1972/73) 293.